Characterizing the nonclassicality of mesoscopic optical twin-beam states

Alessia Allevi*
Dipartimento di Scienza e Alta Tecnologia, Università degli Studi dell'Insubria, I-22100 Como, Italy and CNISM UdR Como, I-22100 Como, Italy

Marco Lamperti
Dipartimento di Scienza e Alta Tecnologia, Università degli Studi dell'Insubria, I-22100 Como, Italy

Maria Bondani
Istituto di Fotonica e Nanotecnologie, CNR-IFN, I-22100 Como, Italy and CNISM UdR Como, I-22100 Como, Italy

Jan Peřina, Jr. and Václav Michálek
Institute of Physics of Academy of Sciences of the Czech Republic, Joint Laboratory of Optics of Palacký University, 17. listopadu 12, 772 07 Olomouc, Czech Republic

Ondřej Haderka and Radek Machulka
RCPTM, Joint Laboratory of Optics of Palacký University and Institute of Physics of Academy of Sciences of the Czech Republic, Faculty of Science, Palacký University, 17. listopadu 12, 77146 Olomouc, Czech Republic

(Received 31 July 2013; published 2 December 2013)

We present a robust tool to analyze nonclassical properties of multimode twin-beam states in the mesoscopic photon-number domain. The measurements are performed by direct detection. The analysis exploits three different nonclassicality criteria for detected photons exhibiting complementary behavior in the explored intensity regime. Joint signal-idler photon-number distributions and quasidistributions of integrated intensities are determined and compared with the corresponding distributions of detected photons. Experimental conditions optimal for nonclassical properties of twin-beam states are identified.

DOI: 10.1103/PhysRevA.88.063807 PACS number(s): 42.50.Ar, 42.50.Dv, 42.65.Lm, 85.60.Gz

I. INTRODUCTION

Quantum nature of an optical state is mandatory for exploiting the state in many useful applications including those in quantum information and metrology [1–5]. By definition, a state is nonclassical whenever it cannot be written as a positive superposition of coherent states. Using the Glauber-Sudarshan representation of a statistical operator [6,7], nonclassical states are described by negative or even singular probability P functions (quasidistributions). However, as P functions introduced in this representation cannot be directly observed, also other nonclassicality criteria based on measurable quantities have been derived [8–12]. For instance, the negativity of the Wigner function of a state available experimentally is commonly used as a nonclassicality indicator [13–15]. Unfortunately, this function is defined only for single-mode states and so it cannot be used to describe the usual spectrally and spatially multimode fields [16,17]. Moreover, the retrieval of Wigner function, typically obtained through optical homodyne tomography, is in general challenging as it requires optimal spatiotemporal matching between the state under investigation and a local oscillator [18–20].

An alternative approach to investigate the quantum properties of a state is provided by the direct detection of the number of photons in the state. Direct detection offers the possibility to reconstruct the photon-number distribution and evaluate possible correlations between the components of a bipartite state [21–23]. The nonclassicality of a photon-number distribution can be indicated by the values of its Fano factor $F = \sigma^2(n)/\langle n\rangle$ (σ^2 and $\langle\ \rangle$ stand for variance and mean value, respectively): $F < 1$ means nonclassical sub-Poissonian statistics [24,25]. On the other hand, when a bipartite state exhibits photon-number correlations, a noise reduction factor $R = \sigma^2(n_1 - n_2)/\langle n_1 + n_2\rangle$ (n_1 and n_2 are the signal and idler photon numbers) having values lower than 1 indicates nonclassicality [26–30].

As one has no direct access to photons, it is of paramount importance to define nonclassicality criteria in terms of detected photons. In fact, the introduction and exploitation of nonclassicality conditions for measurable quantities give the possibility to avoid the use of photon-number reconstruction methods that are in general complex. In this paper, we experimentally investigate optical multimode twin-beam (TWB) states containing sizable numbers of photon pairs. We report on the characterization of their quantumness by means of a direct detection scheme involving two photon-counting detectors that are able to operate in the mesoscopic photon-number domain, in which more than one pair of photons is produced at each laser shot. In particular, we compare three different nonclassicality criteria based on detected photon-number correlations and discuss the conditions suitable for their application. Moreover, we compare these criteria with the genuine definition of nonclassicality using both the measured joint signal-idler detected-photon distributions and reconstructed joint signal-idler photon-number distributions and the corresponding quasidistributions of integrated intensities [31].

*alessia.allevi@uninsubria.it

Even if the overall detection efficiency of our apparatus is relatively low, we demonstrate that quantities determined for detected photons are sufficient to reveal the quantum features of the generated TWB states. The presented comprehensive approach can thus be considered as a robust tool for discriminating nonclassical TWB states in different experimental regimes.

The paper is organized as follows. The experimental setup is described in Sec. II. Nonclassical characteristics of twin beams derived for detected photons are analyzed in Sec. III. Section IV is devoted to the reconstruction of joint signal-idler photon-number distributions, the determination of quasidistributions of integrated intensities, and their nonclassical features. Conclusions are drawn in Sec. V.

II. EXPERIMENTAL IMPLEMENTATION OF MULTIMODE TWB STATES

According to the experimental setup shown in Fig. 1, mesoscopic TWB states were obtained in spontaneous parametric down-conversion (SPDC) in a nonlinear crystal with $\chi^{(2)}$ susceptibility. In particular, we sent the third harmonics (at 266 nm) of a cavity-dumped Kerr-lens mode-locked Ti:sapphire laser (Mira 900, Coherent Inc. and PulseSwitch, A.P.E.) to a type-I β-BaB_2O_4 crystal (BBO hereafter, $8 \times 8 \times 5$ mm^3, cut angle $\vartheta_c = 48^\circ$) tuned for slightly noncollinear interaction geometry. 100-fs long pump-beam pulses were delivered at frequency 11 kHz.

The TWB states generated by the apparatus are intrinsically multimode, both in spatial and spectral domains. By assuming that the output energy is equally distributed among μ modes in each beam, the overall multimode state can be written as a tensor product of μ identical single-mode twin-beam states [32–35], i.e.,

$$|\psi_\mu\rangle = \sum_{n=0}^{\infty} \sqrt{p_n^\mu}\, |n^\otimes\rangle \otimes |n^\otimes\rangle, \tag{1}$$

where $|n^\otimes\rangle = \delta(n - \sum_{h=1}^{\mu} n_h) \otimes_{k=1}^{\mu} |n_k\rangle$ represents an n-photon state coming from μ equally populated modes that impinge on the detector and

$$p_n^\mu = \frac{(n+\mu-1)!}{n!(\mu-1)!(N/\mu+1)^\mu(\mu/N+1)^n} \tag{2}$$

is a multimode thermal photon-number distribution having $N = \langle n \rangle$ mean photons [36]. The TWB state in Eq. (1) exhibits photon-number correlations that are provided by pairwise character of SPDC. To investigate the nature of such correlations and describe their properties, we collected two frequency-degenerate (at 532 nm) parties of the TWB state using two symmetric cage systems. The light in each arm was spectrally filtered by a bandpass filter at high transmissivity, spatially selected by an iris with variable aperture, focused by a lens ($f = 30$ mm) into a multimode fiber (600-μm-core diameter) and delivered to the photodetector. In particular, we used a pair of hybrid photodetectors (HPD, mod. R10467U-40, Hamamatsu, Japan). These detectors are composed of a photocathode, whose quantum efficiency is about 50% in the investigated spectral region [37,38], followed by an avalanche diode operated below breakdown threshold. The internal amplification has a gain profile narrow enough to allow photon-number resolution. The output of each HPD was amplified (preamplifier A250 plus amplifier A275, Amptek), synchronously integrated (SGI, SR250, Stanford), and digitized (ADC, PCI-6251, National Instruments). To perform a systematic characterization of the generated TWB states, each experimental run was repeated 200 000 times for fixed choices of pump mean power and iris sizes.

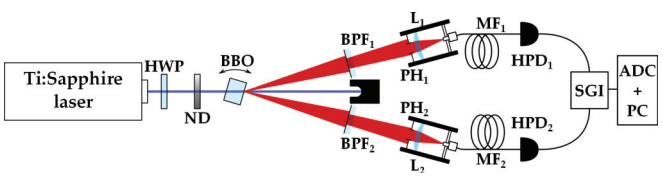

FIG. 1. (Color online) Scheme of the experimental setup. HWP: half wave plate; ND: neutral density filter; BBO: nonlinear crystal; BPF_j: bandpass filter; PH_j: iris with variable aperture; L_j: lens; MF_j: multimode fiber; HPD_j: hybrid photodetector.

III. NONCLASSICAL CHARACTERISTICS OF DETECTED PHOTONS

By exploiting the self-consistent analysis method extensively described in [37,39], we processed the output of each detection chain, obtained detected-photon-number distributions, and evaluated shot-by-shot photon-number correlations. In accordance with Eq. (2) and by taking into account invariance of the functional form of statistics under Bernoullian detection [40], the detected photon-number distributions are described by multimode thermal distributions, in which the number of modes can be determined as $\mu = \langle m \rangle^2/[\sigma^2(m) - \langle m \rangle]$ [34,38], where m is the number of detected photons. Note that $\langle m \rangle = \eta \langle n \rangle$, where η is the detection efficiency. In Fig. 2 we plot the experimental detected-photon-number distributions in the signal arm for three different values of the pump-beam

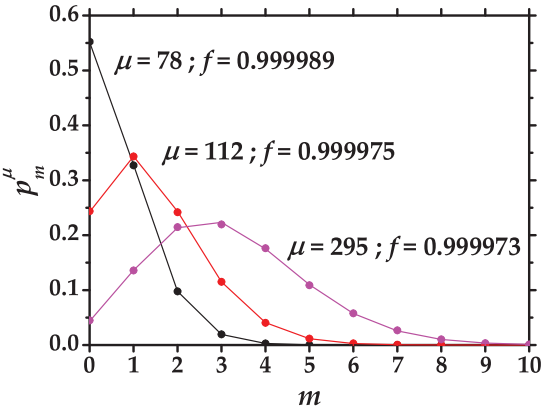

FIG. 2. (Color online) Experimental detected-photon-number distribution in the signal arm for three different values of pump mean power (black dots: 49.2 μW, $\langle m \rangle = 0.60$, and $\mu = 78$; red dots: 118.1 μW, $\langle m \rangle = 1.42$, and $\mu = 112$; magenta dots: 258.3 μW, $\langle m \rangle = 3.14$, and $\mu = 295$) for the fixed value of iris sizes (46 mm^2); lines: theoretical expectations. Fidelities in the figure are calculated as $f = \sum_m \sqrt{p^\mu_{m,\mathrm{expt}} p^\mu_{m,\mathrm{theor}}}$, where the subscript expt (theor) denotes experimental (theoretical) distributions. Error bars are smaller than the symbol sizes.

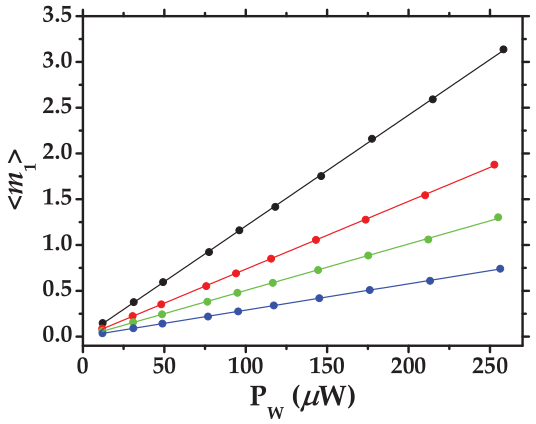

FIG. 3. (Color online) Mean number of detected photons in the signal arm as a function of pump mean power P_W for different values of iris sizes (from top to bottom, black: 45.92 mm^2; red: 20.58 mm^2; green: 10.63 mm^2; blue: 5.67 mm^2). Dots: experimental data; lines: linear fitting curves.

power keeping fixed the value of iris size (dots). Lines are the expected theoretical curves obtained from Eq. (2) by replacing N by the measured mean number of photons. The mean detected-photon numbers presented in Fig. 2 demonstrate the capability of the detection apparatus to capture TWB states in different intensity regimes. Nevertheless, it is worth noting that the SPDC gain is linear in the whole investigated photon-number domain. This is evident in Fig. 3, where we show the mean values of photons detected in the signal arm as functions of the pump mean power for different values of iris sizes.

The observed detected-photon-number correlations were quantified by means of the correlation coefficient

$$C = \frac{\langle m_1 m_2 \rangle - \langle m_1 \rangle \langle m_2 \rangle}{\sqrt{\sigma^2(m_1)\sigma^2(m_2)}} \tag{3}$$

that is plotted in Fig. 4(a) as a function of the value of iris sizes [41]. However, as already demonstrated in [42], the existence of correlations is not sufficient to discriminate between quantum and classical states. For example, bipartite states obtained by dividing classical super-Poissonian states at a beam splitter also display photon-number correlations [43,44]. The noise reduction factor R mentioned above is an explicit marker of nonclassicality originating in photon-number correlations. For detected photons it is determined along the formula

$$R = \frac{\sigma^2(m_1 - m_2)}{\langle m_1 + m_2 \rangle}. \tag{4}$$

It has been shown [45] that whenever the value of R lies in between $1 - \eta$ and 1 [41], the detected state is nonclassical. In this case, we have sub-shot-noise correlations since the fluctuations in the detected photon-number correlations are below the shot-noise level [46–48]. The behavior of R as a function of the value of iris sizes is quantified in Fig. 4(b), in which the nonclassical character of all obtained data is confirmed [49]. To produce the theoretical values shown in Fig. 4, we inserted in Eqs. (3) and (4) the experimental values

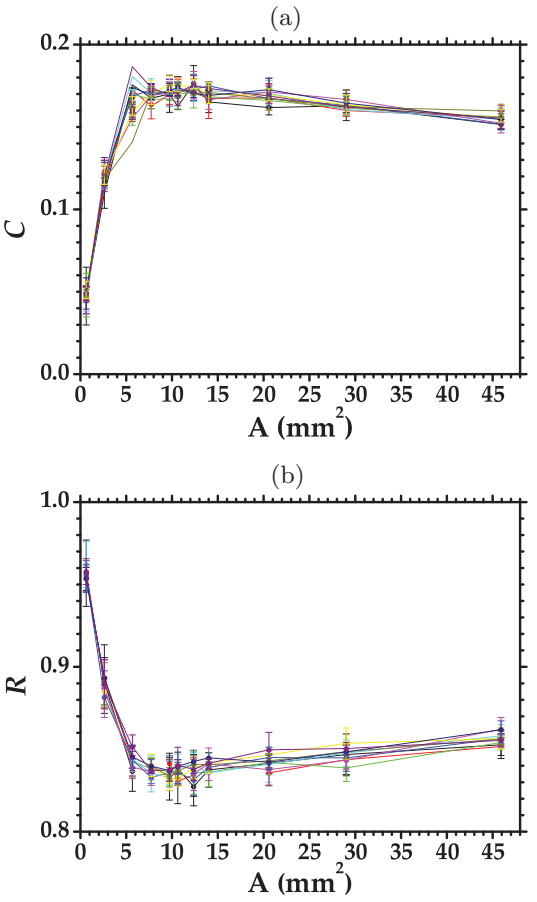

FIG. 4. (Color online) (a) Intensity correlation coefficient C and (b) noise reduction factor R as functions of iris sizes A for different values (different colors) of pump mean power. Dots: experimental data; lines: theoretical expectations. The lines are used to better guide the eye.

of η, $\langle m_1 \rangle$, $\langle m_2 \rangle$, and μ obtained in a self-consistent way [33] for each considered value of the iris sizes. This results in the irregular behavior of the curve connecting the obtained points in the graphs in Fig. 4. Comparison of the curves in Figs. 4(a) and 4(b) reveals complementary behavior of values of the correlation coefficient C and noise reduction factor R. Moreover, it follows from the curves in Fig. 4(b) that the noise reduction factor R attains its minimum for a certain value of iris sizes.

This occurs when the irises are ∼3 mm wide and select the largest possible portions of the twin-beam cones [50]. This explanation is confirmed by the behavior of mean detected-photon numbers $\langle m_1 \rangle$ in the signal arm depending on the iris sizes. As shown in Fig. 5 the mean detected-photon numbers $\langle m_1 \rangle$ stop increasing linearly with the iris size at the same value. Also the maximum extension of emission cones beyond the filters was reached in the horizontal plane at this value. Further increase in mean detected-photon numbers $\langle m_1 \rangle$ is caused only by additional contributions in the vertical plane.

The values of C and R plotted in Fig. 4 may be divided into three groups depending on different values of iris sizes. For small values of the iris sizes, C and R get smaller and higher values, respectively, as only a small portion of the twin beam is collected. For moderate values of the iris sizes, C and

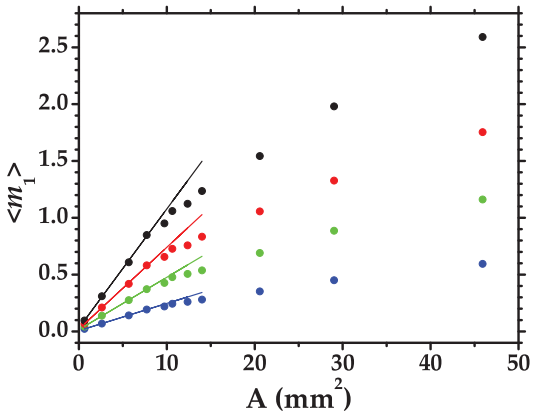

FIG. 5. (Color online) Mean number of detected photons $\langle m_1 \rangle$ in the signal arm as a function of iris sizes A for different values of pump mean power (from top to bottom, black: 215 μW; red: 145 μW; green: 95 μW; blue: 50 μW). Dots: experimental data; lines: linear fitting curves.

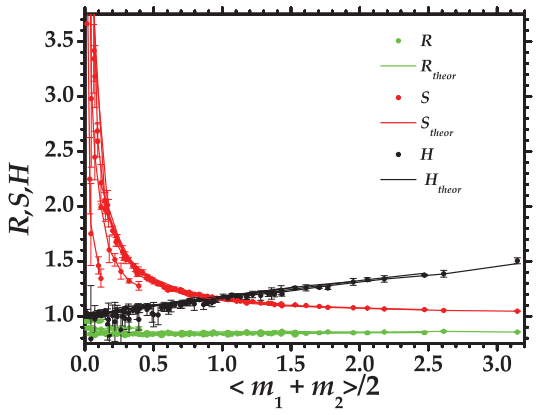

FIG. 6. (Color online) Noise reduction factor R, green color (light gray), Schwarz-inequality factor S, red color (gray), and higher-order-moments factor H, black color (black), as functions of mean number of photons detected in the two arms. Dots: experimental data; lines: theoretical expectations, indicated by subscript theor in the legend.

R reach their highest and smallest values, respectively, due to optimum collection conditions. For large values of the iris sizes, smaller values of C together with greater values of R are observed because the irises exceed the width of the cone.

We discuss advantages and limitations of the noise reduction factor R as a nonclassicality quantifier in comparison with the other two quantities. In particular, we consider a ratio S derived from the Schwarz inequality [51] for detected photons:

$$S = \frac{\langle m_1 m_2 \rangle}{\sqrt{\langle m_1^2 \rangle \langle m_2^2 \rangle}}. \tag{5}$$

If $S > 1$ the state is nonclassical. The second analyzed quantity is determined from a more recent criterion based on higher-order detected-photon-number correlations [33]:

$$H = \langle m_1 \rangle \langle m_2 \rangle \frac{g^{22} - [g^{13}]_s}{g^{11}} + \sqrt{\langle m_1 \rangle \langle m_2 \rangle} \frac{[g^{12}]_s}{g^{11}}, \tag{6}$$

where $g_m^{jk} = \langle m_1^j m_2^k \rangle (\langle m_1 \rangle^j \langle m_2 \rangle^k)^{-1}$ is the $(j+k)$th-order correlation function and $[g^{jk}]_s = (g^{jk} + g^{kj})/2$ represents its symmetrized version. If $H > 1$ the state is nonclassical. In Fig. 6, we show the results obtained by applying the above nonclassicality criteria to the experimental data. The three quantities are plotted as functions of the mean number of photons detected in one of the two arms: good quality of our data is confirmed by the fact that all criteria are satisfied simultaneously. For each criterion the data are distributed into three groups differing in iris sizes, as already mentioned in the description of Fig. 4. It is also interesting to note that all the experimental points (except a very few of them) obtained for different values of pump mean powers and iris sizes are in good agreement with the corresponding theoretical predictions calculated for the actual values of experimental parameters. In particular, the theoretical curve of noise reduction factor R was drawn along the formula

$$R = 1 - 2\eta \frac{\sqrt{\langle m_1 \rangle \langle m_2 \rangle}}{\langle m_1 \rangle + \langle m_2 \rangle} + \frac{(\langle m_1 \rangle \langle m_2 \rangle)^2}{\mu(\langle m_1 \rangle + \langle m_2 \rangle)}, \tag{7}$$

that represents a generalization of the expression derived in [42] to the multimode case. In Eq. (7), μ gives the average of the signal and idler mode numbers, $\langle m_1 \rangle$ and $\langle m_2 \rangle$ are the experimental mean signal and idler detected-photon numbers, and a common quantum detection efficiency η was determined from the formula $R = \sigma^2(m_1 - m_2)/(\langle m_1 \rangle + \langle m_2 \rangle) = 1 - \eta$ valid for an ideal twin beam [33]. As the curves in Fig. 6 document, the values of noise reduction factor R are practically independent of the mean detected-photon numbers. On the other hand, quantities related to the other two nonclassicality criteria depend strongly on the mean detected-photon numbers. Whereas the Schwarz inequality is more suitable for detecting nonclassicality for small mean detected-photon numbers, the inequality based on higher-order moments is preferred for larger mean detected-photon numbers. In fact, this criterion is more sensitive to noise with respect to the other two criteria because of the presence of higher-order moments. As a consequence, when the mean numbers of photons are very low, a lot of acquisitions are required for successful application of this criterion.

IV. NONCLASSICAL CHARACTERISTICS OF THE RECONSTRUCTED PHOTON FIELDS

The generated TWB states are highly nonclassical as they are composed of photon pairs. The amount of their nonclassicality decreases during their propagation towards the detectors as some of photons lose their twins. However, by far the largest loss of nonclassicality occurs during the detection by hybrid photodetectors as their actual overall detection efficiencies lie around 17%, as confirmed by the minimum value achieved by R. Despite this and in accordance with the results of the previous section, even the detected photons exhibit strong pairwise correlations that guarantee nonclassical behavior of the detected-photon fields. Nevertheless, the amount of nonclassicality found in the detected-photon fields is considerably lower compared to that of the original TWB containing photon pairs.

For this reason, it is important to reconstruct the original TWB in terms of photon numbers starting from the experimental detected-photon distributions $f_m(m_s, m_i)$ in order to reveal the quantum nature of state emitted in the nonlinear

process. The reconstructed joint signal-idler photon-number distributions $p(n_s,n_i)$ can be obtained either by applying the maximum-likelihood approach [52–55] or by fitting the experimental detected-photon distributions using a special analytical form of the photon-number distribution $p(n_s,n_i)$ [35,54]. The second approach is more convenient as it allows us to determine also quantum detection efficiencies η_s and η_i of the signal and idler beams, respectively [55]. The method only assumes that the detected nonideal TWB can be decomposed into three statistically independent parts, namely the paired part, the signal noise part, and the idler noise part, which are all described by multimode thermal fields. According to this model, the joint signal-idler photon-number distribution $p(n_s,n_i)$ [34] can be written as

$$p(n_s,n_i) = \sum_{n=0}^{\min[n_s,n_i]} p_{\mathrm{MR}}(n_s-n;\mu_s,b_s) \times p_{\mathrm{MR}}(n_i-n;\mu_i,b_i)p_{\mathrm{MR}}(n;\mu_p,b_p), \tag{8}$$

in which the Mandel-Rice distributions are written as $p_{\mathrm{MR}}(n;\mu,b) = \Gamma(n+\mu)/[n!\,\Gamma(\mu)]b^n/(1+b)^{n+\mu}$ and Γ denotes the Γ function. In Eq. (8), mean photon (photon-pair) numbers per mode b_k and numbers μ_k of independent modes for the paired part ($k=p$), noise signal part ($k=s$), and noise idler part ($k=i$) as suitable characteristics of the analyzed TWBs have been introduced. As the Mandel-Rice distributions in Eq. (8) are defined for arbitrary non-negative real numbers μ of modes, the same applies also to the distribution $p(n_s,n_i)$ in Eq. (8). This allows to consider a broader class of analytic distributions when fitting the experimental data. We note that formula (2) has been derived for an integer number μ of modes, but its generalization to real non-negative μ is straightforward [34].

The photon-number distribution $p(n_s,n_i)$ is related to the theoretical detected-photon distribution $f_{m,\mathrm{theor}}(m_s,m_i)$ by quantum detection efficiencies η_s and η_i [53]. Since detection by hybrid photodetectors is characterized by the Bernoulli distribution, we can express this relation as

$$f_{m,\mathrm{theor}}(m_s,m_i) = \sum_{n_s,n_i=0}^{\infty} B_s(m_s,n_s)B_i(m_i,n_i)p(n_s,n_i) \tag{9}$$

using the Bernoulli coefficients $B_k(m_k,n_k)$,

$$B_k(m_k,n_k) = \binom{n_k}{m_k}\eta_k^{m_k}(1-\eta_k)^{n_k-m_k}. \tag{10}$$

A fitting procedure that minimizes the declination between the experimental histogram $f_m(m_s,m_i)$ and theoretical detected-photon distribution $f_{m,\mathrm{theor}}(m_s,m_i)$ under the assumption of equality of the first and second experimental and theoretical detected photon-number moments (for details, see [31]) allows us to determine both quantum detection efficiencies η_k, $k=s,i$, and parameters b_k and μ_k, $k=p,s,i$, of the analyzed TWB. To give a typical example, we consider the experimental data obtained for pump mean power 49.2 μW and iris size's area 46 mm^2 (see the marginal distribution plotted as black dots in Fig. 2). The fitting procedure assigned the following parameters to the experimental distribution f_m: $\eta_s = 0.147$, $\eta_i = 0.150$, $\mu_p = 31$, $b_p = 0.13$, $\mu_s = 1.2\times10^{-3}$, $b_s = 24$, $\mu_i = 5.5\times10^{-3}$, and $b_i = 13$. First of all, we note that the values of quantum efficiencies obtained by the reconstruction method are comparable with the value obtained from the noise reduction factor for the same set of data [see points at 46 mm^2 in Fig. 4(b)] [56]. Second, we remark that the paired part of TWB representing more than 98% of the entire field is described by a multithermal field with 31 independent modes. We note that the mean number of photons in paired fields equals 8, whereas the means of noisy signal and idler photon numbers lay below 0.1. On the other hand, the noise signal and idler parts have numbers μ of modes much less than 1 which means that their probability densities have appreciated values only very close to the zero photon number. This is a consequence of very low noise signal and idler intensities observed in the experiment. We attribute the found numbers μ of modes much less than 1 to distortions of electronic signals inside the detection chains including HPDs.

Finally, we point out that whereas the joint signal-idler experimental detected-photon histogram f_m provided covariance equal to 0.16, covariance of photon numbers in the reconstructed photon-number distribution p is equal to 0.85. The reconstruction also decreased the value of noise reduction factor R to 0.2. This dramatic increase of correlations between the signal and idler fields in a TWB after the reconstruction also changes the shape of the corresponding joint signal-idler (detected) photon-number distributions (see Fig. 7). In fact, the presence of nonzero off-diagonal elements in the detected photon-number distribution in Fig. 7(a) makes its nonclassical character less evident compared to the reconstructed photon-number distribution $p(n_s,n_i)$ plotted in Fig. 7(b) and clearly showing the prevailing pairwise character of the TWB (the off-diagonal elements attain values lower than 1% of those of diagonal elements). Also, the sum of diagonal elements gives 98.2% of the entire joint signal-idler photon-number distribution. This is in accord with the relative weights of paired, noise signal, and noise idler parts of the TWB expressed in mean pair-photon numbers. A substantial difference in the nonclassical behavior of detected-photon-number and photon-number distributions can be observed in the corresponding distributions of the sum and difference of the signal and idler detected-photon and photon numbers, respectively. The resulting distributions are compared with those obtained by the combination of two independent classical fields with Poissonian statistics. This comparison applied to the experimental detected-photon distribution reveals only weak signatures of nonclassicality in the distributions $f_{m,+}(m_s+m_i)$ and $f_{m,-}(m_s-m_i)$ of the sum m_s+m_i and difference m_s-m_i of the signal and idler detected-photon numbers defined as

$$\begin{aligned} f_{m,+}(m) &= \sum_{m_s,m_i=0}^{\infty} \delta_{m,m_s+m_i} f_m(m_s,m_i), \\ f_{m,-}(m) &= \sum_{m_s,m_i=0}^{\infty} \delta_{m,m_s-m_i} f_m(m_s,m_i), \end{aligned} \tag{11}$$

where δ denotes the Kronecker symbol. As shown in Fig. 8(a), the experimental distribution $f_{m,-}(m_s-m_i)$ of the difference is slightly narrower than the reference distribution. On the other hand, a slightly broader experimental distribution $f_{m,+}(m_s+m_i)$ of the sum with respect to the reference distribution is drawn in Fig. 9(a). The reconstruction of joint

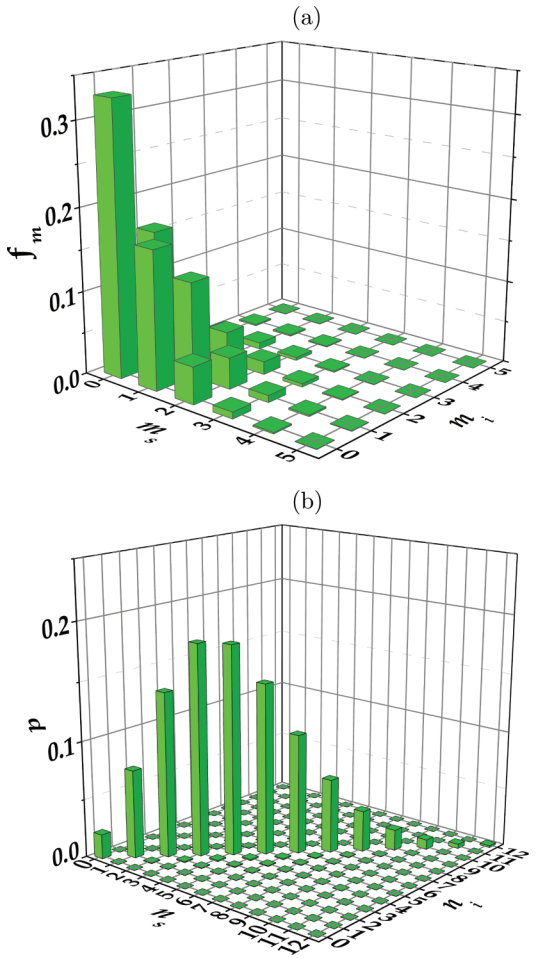

FIG. 7. (Color online) (a) Experimental joint signal-idler detected photon-number distribution $f_m(m_s,m_i)$ and (b) reconstructed joint signal-idler photon-number distribution $p(n_s,n_i)$ for the pump power 49.2 μW.

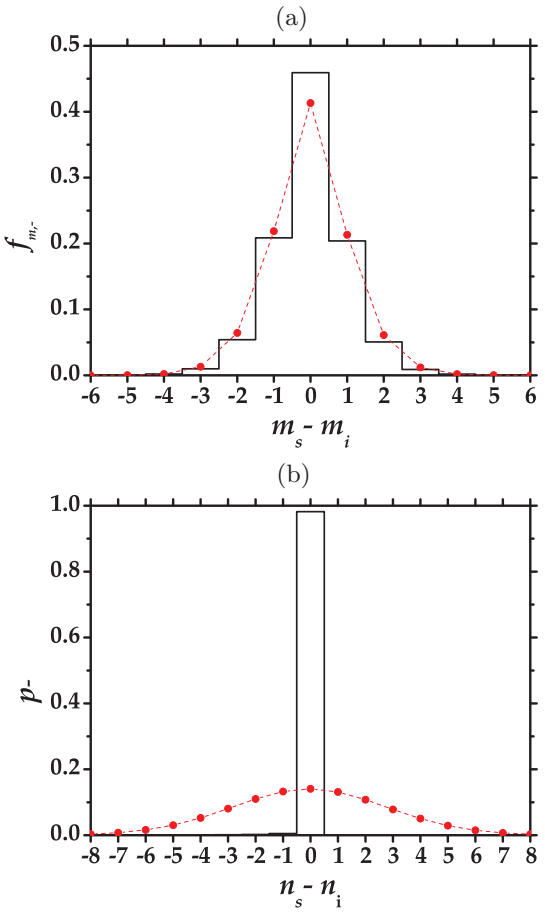

FIG. 8. (Color online) (a) Detected photon-number distribution $f_{m,-}(m_s - m_i)$ (bars) and (b) photon-number distribution $p_-(n_s - n_i)$ (bars) of the difference between signal and idler detected-photon and photon numbers, respectively, for the data shown in Fig. 7. In the two panels we also show the distributions obtained by the combination of two independent classical fields with Poissonian statistics (dashed line + symbols).

photon-number distribution clearly reveals nonclassicality of TWBs, as documented by the photon-number distributions $p_-(n_s - n_i)$ and $p_+(n_s + n_i)$ plotted in Figs. 8(b) and 9(b). The distribution $p_-(n_s - n_i)$ of photon-number difference plotted in Fig. 8(b) demonstrates the prevailing pairwise character of TWBs that is also confirmed by a "teethlike" character of the photon-number distribution $p_+(n_s + n_i)$ of the photon-number sum depicted in Fig. 9(b).

An ultimate criterion for discriminating quantum and classical multimode fields is related to the properties of quasidistribution P of integrated intensities, i.e., electric-field intensities integrated over the detection interval, related to normal ordering of field operators (for more details, see, e.g., [24,34,57]). The reason is that integrated intensities describe the fields before detection that may conceal nonclassical features of these fields. The relation between integrated intensities and detected photons is provided by Mandel's detection formula [24]. This formula can be inverted [34] and then used for the determination of quasidistributions of integrated intensities from the photon-number distributions obtained from experimental data. According to quantum theory of radiation [34,58] if the quasidistribution P attains negative values or is even singular, the field is nonclassical.

The quasidistribution $P(W_s,W_i)$ of signal (W_s) and idler (W_i) integrated intensities can be written in the form of twofold convolution, which is a consequence of Eq. (8) for the photon-number distribution $p(n_s,n_i)$ [31]:

$$P(W_s,W_i) = \int_0^\infty dW_s' \int_0^\infty dW_i' P_p(W_s - W_s', W_i - W_i') \times P_s(W_s') P_i(W_i'). \quad (12)$$

Quasidistributions P_k of integrated intensities introduced in Eq. (12) describe the paired ($k = p$), signal noise ($k = s$), and idler noise ($k = i$) parts of the TWB. More details can be found in [31,35].

As we have demonstrated, many nonclassicality criteria indicate quantum behavior of even experimental distributions written in terms of detected photons. Following the genuine definition of nonclassicality, we can define a quasidistribution P_m of "detected-photon intensities" following the approach developed for photons and assuming perfect quantum detection efficiencies ($\eta_s = \eta_i = 1$) [29]. Of course, the obtained quasidistribution P_m characterizes a fictitious

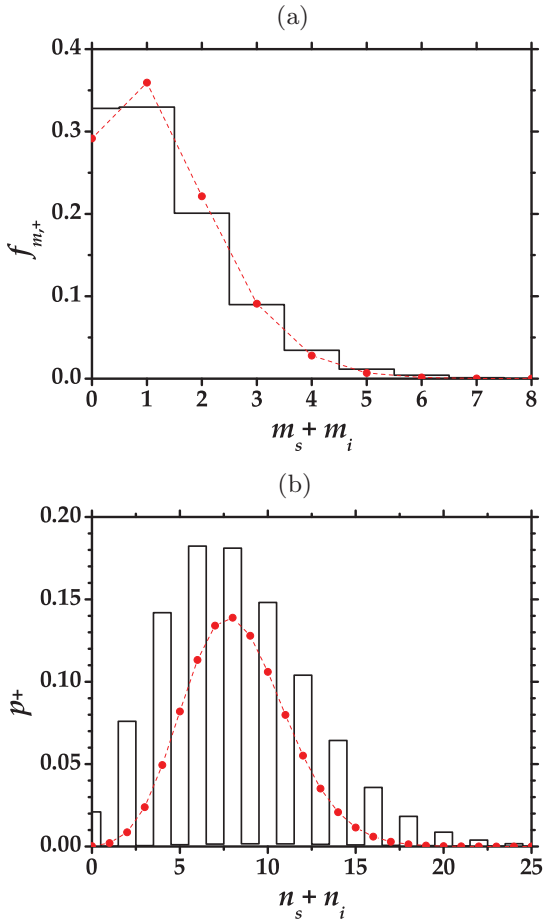

FIG. 9. (Color online) (a) Detected photon-number distribution $f_{m,+}(m_s + m_i)$ (bars) and (b) photon-number distribution $p_+(n_s + n_i)$ (bars) of the sum of signal and idler detected-photon and photon numbers, respectively, for the data shown in Fig. 7. In the two panels we also show the distributions obtained by the combination of two independent classical fields with Poissonian statistics (dashed line + symbols).

"detected-photon" boson field, as it contains only those photons that are captured by the detectors. As in the case of quasidistribution of integrated intensities, the existence of negative regions in the quasidistribution P_m for detected photons confirms the nonclassical character of the state. The quasidistribution $P_m(W_s, W_i)$ of detected-photon intensities determined from the analyzed experimental distribution f_m is shown in Fig. 10. In order to see a detained behavior of this quasidistribution and in particular to investigate in which regions it attains values close to zero, we plot only a part of the function in Fig. 10(a) and remark that the maximum of the peak in the origin reaches the value 7×10^5. The smallest negative values, equal to -0.2, are found close to the W_s and W_i axes. The highly prevailing positive part of quasidistribution P_m indicates that the measured state is close to a classical one. However, the presence of a negative part (even small) shows that the low detection efficiency has preserved the pairwise character of TWB. The comparison of the quasidistribution P_m of detected-photon intensities with the genuine quasidistribution P of photon intensities [see Fig. 10(c)] reveals much stronger nonclassicality in the case

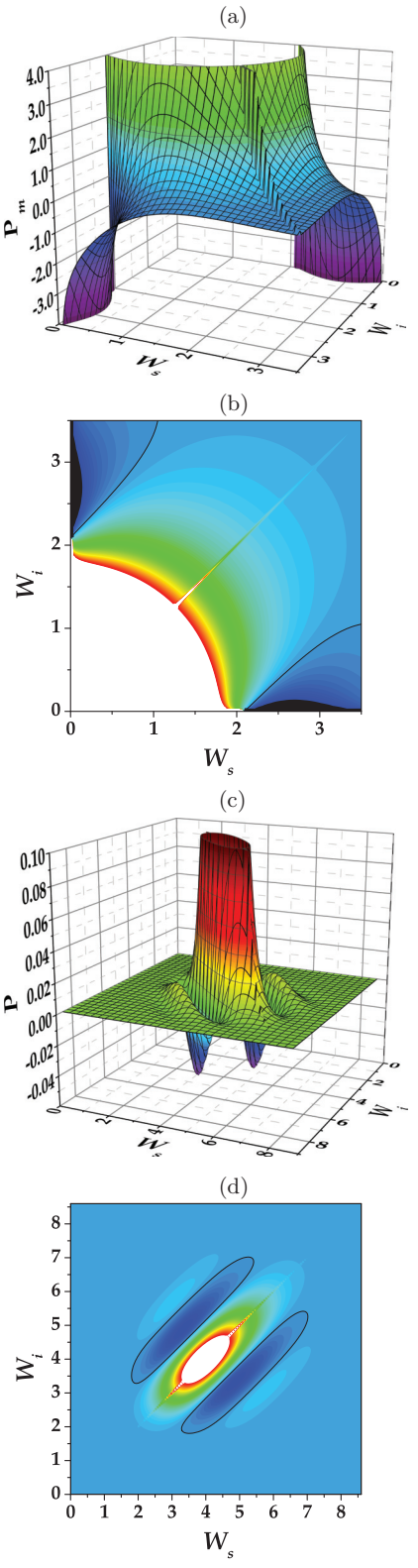

FIG. 10. (Color online) (a) Quasidistribution of "detected-photon intensities" $P_m(W_s, W_i)$ and its topograph, (b). (c) Quasidistribution of photon integrated intensities $P(W_s, W_i)$ and its topograph, (d). Topo graphs in (b) and (d) have the same scales as in (a) and (c), respectively. In (b) and (d) black contours mark the zero level.

of photons. We note that the peak value of P in Fig. 10(c) equals 0.99 which is considerably lower than the peak value

of quasidistribution P_m shown in Fig. 10(a). Nevertheless, both quasidistributions attain negative values and so both describe a nonclassical field. The contour plots of both quasidistributions depicted in Figs. 10(b) and 10(d) reveal that negative values of these distributions are localized in parallel strips whose orientation originates in the pairwise character of TWBs.

V. CONCLUSIONS

Using SPDC in the linear gain regime, we generated multimode twin-beam states in the mesoscopic photon-number regime. We studied nonclassical properties of the twin beams by applying three different nonclassicality criteria written in terms of detected photons. Whereas the noise reduction factor R is a suitable indicator of nonclassicality independent of the twin-beam intensity, the Schwarz inequality is useful for weak twin beams and the criterion derived from higher-order detected-photon-number moments finds its application for intense twin beams. To compare these criteria with the genuine definition of nonclassicality we also determined quasidistributions of detected-photon and photon integrated intensities for normally ordered field operators. Despite the low detection efficiency (around 17%) negative values of these quasidistributions found in typical strips were observed both for photons and detected photons, confirming nonclassicality of the generated twin beams. The set of criteria we presented can thus be considered as a robust tool for quantifying nonclassicality of multimode twin beams used in many schemes, including that for conditional generation of nonclassical and non-Gaussian states.

ACKNOWLEDGMENTS

The research leading to these results has been supported by MIUR (FIRB LiCHIS - RBFR10YQ3H). Support by projects P205/12/0382 of GA ČR, Operational Program Research and Development for Innovations - European Regional Development Fund project CZ.1.05/2.1.00/03.0058, and Operational Program Education for Competitiveness - European Social Fund project CZ.1.07/2.3.00/20.0058 of MŠMT ČR are acknowledged.

[1] M. S. Kim, W. Son, V. Bužek, and P. L. Knight, Phys. Rev. A **65**, 032323 (2002).
[2] S. L. Braunstein and P. van Loock, Rev. Mod. Phys. **77**, 513 (2005).
[3] I. A. Walmsley and M. G. Raymer, Science **307**, 1733 (2005).
[4] T. C. Ralph, Rep. Prog. Phys. **69**, 853 (2006).
[5] P. Kok, W. J. Munro, K. Nemoto, T. C. Ralph, J. P. Dowling, and G. J. Milburn, Rev. Mod. Phys. **79**, 135 (2007).
[6] R. J. Glauber, Phys. Rev. **131**, 2766 (1963).
[7] E. C. G. Sudarshan, Phys. Rev. Lett. **10**, 277 (1963).
[8] D. N. Klyshko, Phys. Lett. A **213**, 7 (1996).
[9] Th. Richter and W. Vogel, Phys. Rev. Lett. **89**, 283601 (2002).
[10] A. Zavatta, V. Parigi, and M. Bellini, Phys. Rev. A **75**, 052106 (2007).
[11] A. Miranowicz, M. Bartkowiak, X. Wang, Y.-X. Liu, and F. Nori, Phys. Rev. A **82**, 013824 (2010).
[12] G. Brida, M. Bondani, I. P. Degiovanni, M. Genovese, M. G. A. Paris, I. Ruo Berchera, and V. Schettini, Found. Phys. **41**, 305 (2011).
[13] A. I. Lvovsky, H. Hansen, T. Aichele, O. Benson, J. Mlynek, and S. Schiller, Phys. Rev. Lett. **87**, 050402 (2001).
[14] A. Zavatta, S. Viciani, and M. Bellini, Science **306**, 660 (2004).
[15] A. Ourjoumtsev, R. Tualle-Brouri, and P. Grangier, Phys. Rev. Lett. **96**, 213601 (2006).
[16] A. I. Lvovsky, W. Wasilewski, and K. Banaszek, J. Mod. Opt. **54**, 721 (2007).
[17] W. Mauerer, M. Avenhaus, W. Helwig, and C. Silberhorn, Phys. Rev. A **80**, 053815 (2009).
[18] W. Wasilewski, A. I. Lvovsky, K. Banaszek, and C. Radzewicz, Phys. Rev. A **73**, 063819 (2006).
[19] A. Zavatta, S. Viciani, and M. Bellini, Laser Phys. Lett. **3**, 3 (2006).
[20] C. Polycarpou, K. N. Cassemiro, G. Venturi, A. Zavatta, and M. Bellini, Phys. Rev. Lett. **109**, 053602 (2012).
[21] O. A. Ivanova, T. Sh. Iskhakov, A. N. Penin, and M. V. Chekhova, Quantum Electron. **36**, 951 (2006).
[22] M. Avenhaus, K. Laiho, M. V. Chekhova, and C. Silberhorn, Phys. Rev. Lett. **104**, 063602 (2010).
[23] A. Christ, K. Laiho, A. Eckstein, K. N. Cassemiro, and C. Silberhorn, New J. Phys. **13**, 033027 (2011).
[24] L. Mandel and E. Wolf, *Optical Coherence and Quantum Optics* (Cambridge University Press, Cambridge, England, 1995).
[25] J. Peřina, Jr., O. Haderka, and V. Michálek, Opt. Express **21**, 19387 (2013).
[26] D. T. Smithey, M. Beck, M. Belsley, and M. G. Raymer, Phys. Rev. Lett. **69**, 2650 (1992).
[27] J. G. Rarity, P. R. Tapster, J. A. Levenson, J. C. Garreau, I. Abram, J. Mertz, T. Debuisschert, A. Heidmann, C. Fabre, and E. Giacobino, Appl. Phys. B **55**, 250 (1992).
[28] J. Wenger, R. Tualle-Brouri, and P. Grangier, Opt. Lett. **29**, 1267 (2004).
[29] J. Peřina, J. Křepelka, J. Peřina, Jr., M. Bondani, A. Allevi, and A. Andreoni, Phys. Rev. A **76**, 043806 (2007).
[30] J. Peřina, J. Křepelka, J. Peřina, Jr., M. Bondani, A. Allevi, and A. Andreoni, Eur. Phys. J. D **53**, 373 (2009).
[31] J. Peřina, Jr., O. Haderka, V. Michálek, and M. Hamar, Phys. Rev. A **87**, 022108 (2013).
[32] A. Allevi, A. Andreoni, F. A. Beduini, M. Bondani, M. G. Genoni, S. Olivares, and M. G. A. Paris, Europhys. Lett. **92**, 20007 (2010).
[33] A. Allevi, S. Olivares, and M. Bondani, Phys. Rev. A **85**, 063835 (2012).
[34] J. Peřina, *Quantum Statistics of Linear and Nonlinear Optical Phenomena* (Kluwer, Dordrecht, 1991).
[35] J. Peřina and J. Křepelka, J. Opt. B: Quantum Semiclass. Opt. **7**, 246 (2005).
[36] F. Paleari, A. Andreoni, G. Zambra, and M. Bondani, Opt. Express **12**, 2816 (2004).

[37] M. Bondani, A. Allevi, A. Agliati, and A. Andreoni, J. Mod. Opt. **56**, 226 (2009).
[38] M. Bondani, A. Allevi, and A. Andreoni, Adv. Sci. Lett. **2**, 463 (2009).
[39] A. Andreoni and M. Bondani, Phys. Rev. A **80**, 013819 (2009).
[40] M. Bondani, A. Allevi, and A. Andreoni, Opt. Lett. **34**, 1444 (2009).
[41] M. Bondani, A. Allevi, G. Zambra, M. G. A. Paris, and A. Andreoni, Phys. Rev. A **76**, 013833 (2007).
[42] A. Agliati, M. Bondani, A. Andreoni, G. De Cillis, and M. G. A. Paris, J. Opt. B: Quantum Semiclass. Opt. **7**, S652 (2005).
[43] A. Allevi, M. Bondani, and A. Andreoni, Opt. Lett. **10**, 1707 (2010).
[44] A. Allevi, F. A. Beduini, M. Bondani, and A. Andreoni, Int. J. Quantum Inf. **9**, 103 (2011).
[45] I. P. Degiovanni, M. Bondani, E. Puddu, A. Andreoni, and M. G. A. Paris, Phys. Rev. A **76**, 062309 (2007).
[46] O. Jedrkiewicz, Y.-K. Jiang, E. Brambilla, A. Gatti, M. Bache, L. A. Lugiato, and P. Di Trapani, Phys. Rev. Lett. **93**, 243601 (2004).
[47] G. Brida, L. Caspani, A. Gatti, M. Genovese, A. Meda, and I. R. Berchera, Phys. Rev. Lett. **102**, 213602 (2009).
[48] G. Brida, M. Genovese, and I. Ruo Berchera, Nat. Photon. **4**, 227 (2010).
[49] M. Lamperti, A. Allevi, M. Bondani, R. Machulka, V. Michálek, O. Haderka, and J. Peřina, Jr., arXiv:1305.5350 [J. Opt. Soc. Am. B (to be published)].
[50] I. N. Agafonov, M. V. Chekhova, and G. Leuchs, Phys. Rev. A **82**, 011801(R) (2010).
[51] W. Vogel and D.-G. Welsch, *Quantum Optics*, 3rd ed. (Wiley-VCH, New York, 2006).
[52] O. Haderka, J. Peřina, Jr., M. Hamar, and J. Peřina, Phys. Rev. A **71**, 033815 (2005).
[53] J. Peřina, Jr., M. Hamar, V. Michálek, and O. Haderka, Phys. Rev. A **85**, 023816 (2012).
[54] J. Peřina and J. Křepelka, Opt. Commun. **265**, 632 (2006).
[55] J. Peřina, Jr., O. Haderka, V. Michálek, and M. Hamar, Opt. Lett. **37**, 2475 (2012).
[56] G. Brida, I. P. Degiovanni, M. Genovese, M. L. Rastello, and I. Ruo-Berchera, Opt. Express **18**, 20572 (2010).
[57] J. Peřina and J. Křepelka, Opt. Commun. **284**, 4941 (2011).
[58] R. J. Glauber, Phys. Rev. Lett. **10**, 84 (1963).